HiSST: 2nd International Conference on
High-Speed Vehicle Science Technology
11–15 September 2022, Bruges, Belgium

RANS Simulations of Various Combustion Modes in a Scramjet Engine

Masatoshi Kodera[1], Sadatake Tomioka[2] and Tohru Mitani[3]

Abstract

In this study, three-dimensional CFD analysis was carried out for a hydrogen fueled scramjet engine tested at the Ramjet Engine Test Facility (RJTF) under Mach 6 flight conditions. As a result, for a fuel equivalence ratio of 0.3, various combustion modes were observed depending on the combustor wall temperature, the working of igniter, the presence of water vapor in airflows as well as initial solutions. Those combustion modes were classified into 4 groups: Partially-anchored, Fully-anchored, Partially-blow-off and Blow-off modes, from the point of view of flame anchor point, and were investigated in detail. In addition, we made several combustion phenomena occurred in the RJTF tests correspond to one of the combustion modes classified.

Keywords: *Scramjet, RANS CFD*

Nomenclature

Da – Damköhler number
G_{FO} – Flame Index
R – Universal gas constant [[J/K/mol]]
T – Temperature [K]
U – Magnitude of velocity vector [m/s]
X_{ig} – Ignition distance [m]
Y – Mass fraction
p – Pressure [atm]
t – Elapse time from initial condition [msec]
u – Streamwise velocity [m/s]
x – Streamwise coordinate
y – Spanwise coordinate
y^+ – Normalized distance from wall
z – Vertical coordinate
ΔF – Thrust increment from no fuel condition [N]
∇ – Gradient
τ_{ig} – Ignition delay time [s]
τ_R – Reaction time [s]
φ – Local equivalence ratio
$[O_2]$ – Oxygen mole concentration [mol/cm^3]

Subscripts
H_2 – Hydrogen
O_2 – Oxygen
ad – Adiabatic wall
wc – Combustor/nozzle wall

1. Introduction

Japan Aerospace Exploration Agency (JAXA) has prototyped several types of subscale scramjet engines and conducted combustion tests at the Ramjet Engine Test Facility (RJTF) in the Kakuda Space Center [1][2]. RJTF can simulate airflow conditions equivalent to flight Mach numbers of 4, 6 and 8. Especially for the Mach 6 conditions, interesting combustion phenomena were observed in the RJTF tests, since the conditions are close to the self-ignition limit and two types of airflow modes, namely the S and V modes, in which thermal storage and H_2/O_2 combustion heaters are used respectively, can be selected for generating high enthalpy flows. In the S mode, basically clean air is provided, while in the V mode, vitiated air containing water vapor and a small amount of radical is provided, probably affecting combustion.

[1] *Japan Aerospace Exploration Agency, Kakuda, Miyagi 981-1525 JAPAN, kodera.masatoshi@jaxa.jp*
[2] *Japan Aerospace Exploration Agency, Kakuda, Miyagi 981-1525 JAPAN, tomioka.sadatake@jaxa.jp*
[3] *Former Japan Aerospace Exploration Agency*

Regarding Mach 6 RJTF test results, Kanda et al. reported two types of combustion modes: "weak combustion" and "intensive combustion" whose thrust levels differed discontinuously depending on injected fuel flow rates, when conducting combustion tests for a H_2 fueled engine with a side wall compression type inlet named "E1" in the S mode [3]. Mitani et al. compared between the test results of the S and V modes for the same engine and showed that the ignition performance in the V mode was higher probably due to the presence of radicals in the airflow [4]. They also suggested that the combustion was not completely mixing-controlled because of the different combustion characteristics in the two airflow modes. Moreover, from the distributions of local equivalent ratio and combustion efficiency obtained from gas sampling at the engine exit, they concluded that the weak combustion was caused by self-ignition within the boundary layers. In the same comparison, Tomioka et al. focused on the fact that in the intensive combustion, pressure rise due to combustion located more downstream in the V mode compared to the S mode. From a quasi-one-dimensional analysis, they claimed that the causes included the higher enthalpy of the airflow and slower reaction in the V mode [5].

As for CFD studies, Kouchi et al. investigated the transition mechanism between the weak combustion and the intensive combustion by conducting three-dimensional CFD analysis under the S mode conditions corresponding to the RJTF combustion test on the engine E2, which is similar to E1 [6]. They demonstrated by numerical experiments that when forced ignition is done in the weak combustion mode, the boundary layer separates and the combustion zone expands throughout the combustor, transitioning to the intensive combustion. For Tomioka et al.'s study [5], the authors proceeded to further elucidate the reason for the difference between the two airflow modes by three-dimensional CFD analysis as well as one-dimensional analysis [7]. The results revealed that thermal choking didn't occur for the S mode, although initially it was supposed that the pressure distribution greatly changed from the V mode due to it. In addition, they argued that one of the causes for the difference was certainly the thermodynamic effect of the water vapor for the V mode. Moreover, they showed that the combustion might be different between the S and V modes because the premixed and diffusion flames were intermingled near the fuel injector.

Related to the above CFD analysis [7], various combustion modes were observed according to engine wall temperatures, turning on or off the igniter and the existence of water vapor in the airflow as well as initial conditions. Hence, in this study, we will categorize the combustion modes obtained from the CFD results into several groups and scrutinize them. Moreover, we will make some of each group correspond to the RJTF results.

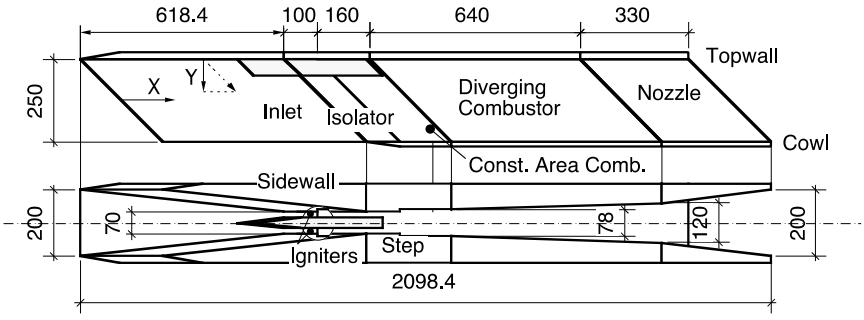

Fig 1. Schematic diagram of E1 engine

2. Approaches

Fig. 1 shows a schematic diagram of the E1 engine analyzed in this study. The engine consists of a pair of side walls forming a compression part inclined at 6 degrees and an expansion part, a flat top wall, and a cowl. The overall length is 2.1 m, and the entrance and exit are 250 mm in height and 200 mm in width. The configuration is so-called "Langley type". The engine is swept back at an angle of 45 degrees overall, facilitating the starting due to air spillage from the inlet where the bottom is open. To avoid the inlet/combustor interaction, a constant cross-sectional area isolator with a length of 100 mm is placed between them. The combustor consists of a constant cross-sectional area combustor (C. C.) and a diverging combustor (D. C.), being followed by an internal nozzle. There are backward facing steps for flame holding between the isolator and combustor on the top and side walls with a height of 2 and 4 mm respectively. Twelve main injector holes with a diameter of 1.5 mm are placed 32 mm

downstream of the step on both the side walls. From the injector, gaseous hydrogen fuel with room temperature is injected into the direction normal to the wall at the speed of sound. Moreover, a 50 mm heigh strut is installed on the top wall to compensate for the lack of compression at the inlet. To make a pilot flame, six sub-injector holes with a diameter of 0.5 mm are also placed at 50 mm upstream of the step on the top wall. Twin plasma jet (PJ) igniters, each with a power of 2.5 kW, are also located on the top wall at 30 mm downstream of the pilot injector one by one at both sides of the strut.

In this study, we used an in-house RANS CFD code based on the unstructured grid method, which has many achievements in combustion flow analysis in the JAXA scramjet engines [8]. The governing equations are the conservations of mass, momentum, energy, and each chemical species, being discretized by the finite volume method. The LU-SGS implicit method is applied to time integration. At the time, a diagonal point implicit method is performed to avoid excessive calculation time and stiffness. The AUSM-DV method [9] is used for evaluation of the inviscid flux. The turbulence model is the one-equation model of Spalart and Allmaras [10] with compressibility correction terms for mixing layers [11]. For hydrogen-air combustion, a reduced reaction mechanism with 9 species and 17 reactions based on that developed by Stahl and Warnatz [12] is adopted.

Table 1. Airflow conditions

		S	V
Mach number		5.30	5.15
Velocity	[m/s]	1620.7	1746.5
Static pressure	[kPa]	5.3	5.8
Static temperature	[K]	232	271
Density	[kg/m^3]	0.07929	0.06987
Stag. pressure	[MPa]	4.78	4.52
Stag. temperature	[K]	1480	1530
O_2 mass fraction		0.234	0.251
H_2O mass fraction		0.000	0.114
N_2 mass fraction		0.766	0.635

Table 2. Numerical conditions for each case and obtained combustion modes

Case	Air	T_{wc} [K]	Initial solution	PJ	Combustion mode
A	S	300	Air only	on	PA
B	S	300	Air only	off	BO
C	S	T_{ad}	Air only	on	FA
D	S	T_{ad}	Air only	off	BO
E	S	300	Case C	on	FA
F	V	300	Air only	on	PA
G	V	300	Air only	off	BO
H	V	T_{ad}	Air only	on	FA
I	V	T_{ad}	Air only	off	PB
J	V	300	Case H	on	FA
K	V	300	Case I	off	PB

Table 1 shows airflow conditions for RJTF Mach 6 tests applying to this study. There are the S and V modes as mentioned before. In addition, in the RJTF test, the boundary layer of the facility nozzle enters the top wall side of the engine, and its displacement thickness is 19.7 mm. The boundary layer profile was obtained by computing a two-dimensional flat plate boundary layer. The total fuel flow rates are 50.5 g/s and 50.4 g/s for the S and V mode conditions respectively. Among them, the fuel flow rates from the pilot injector are 2.4 g/s and 5.4 g/s for the S and V mode conditions respectively. Since the captured mass flow rate is the same between the two airflow conditions, the total fuel equivalence ratio is also the same, and is 0.3. The PJ igniter conditions are the same as the ones used in Takita's

study [13], where a similar configuration of PJ igniter was used. The feedstock of PJ is oxygen. The baseline wall temperature is 300 K, while it is adiabatic one (T_{ad}) in the combustor and nozzle sections in some cases. Table 2 shows parameter sets including the airflow mode (S or V), the combustor/nozzle wall temperature (T_{wc}), initial conditions and the working of the PJ igniter (PJ-on or PJ-off) for all the cases tested in this study. For the time step, a constant time step of 2×10^{-8} sec (1×10^{-8} sec in some cases) is applied to the combustion calculations. The computational domain is only a half side from the engine symmetry plane. The origin of the coordinate system, for which x, y and z axes are in the streamwise, spanwise and vertical directions respectively, is the intersection between the top wall leading edge and symmetry plane. A commercial software named Pointwise [14] is used for grid generation. Prism grid is placed near the wall and the minimum height on the wall and stretching factor away from the wall are 5 μm (average $y^+\approx1$) and 1.1 respectively. The total number of grid points is approximately 9 million. All the calculations were performed on JAXA Supercomputer System generation 2 (JSS2).

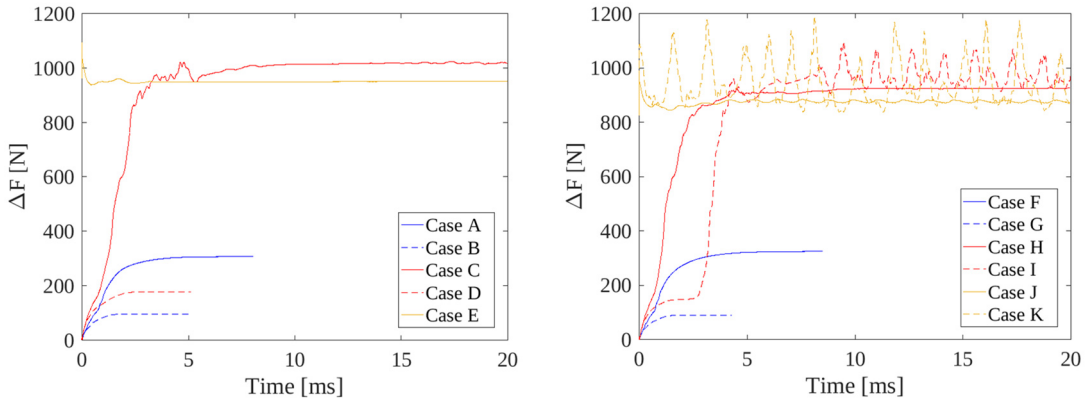

(a) S mode (b) V mode

Fig 2. Time history of thrust increment from no fuel condition

3. Results and discussions

Fig. 2 shows the time history of thrust increment, ΔF, from air only (no fuel) conditions for all the cases as shown in Table 2. The horizontal axis indicates an elapse time from the initial condition (initial solution in Table 2) (t). The variation of ΔF and its convergence value are largely different between the cases, although the fuel equivalence ratio is the same, suggesting the existence of various combustion modes. It is well known that the diffusion flame is dominant in scramjet combustion. Therefore, the spread of combustion regions depends on how to anchor combustion so that the combustion modes observed in this study can be classified into 4 groups: Partially-anchored (PA), Fully-anchored (FA), Partially-blow-off (PB) and Blow-off (BO) modes. Table 2 also shows the results for the classification.

3.1. Partially-anchored and fully-anchored modes

In Fig.2, for the case at the PJ-on and T_{wc}=300 K, ΔF is about 300 N, whereas at $T_{wc} = T_{ad}$, it increases up to nearly 1000 N in some cases (Case A vs. C or Case F vs. H). To investigate the difference, the distributions of Mach number and temperatures on the y=0 m plane (the symmetry plane) and the y=0.025 m plane (a plane between the strut and side wall) for Case A and C are shown in Fig. 3. Here, sonic lines are depicted by black lines on the figures. The temperature distribution shows that for Case A, principal combustion regions exist only within top wall boundary layers, meaning the PA mode. On the other hand, for Case C, the main combustion spreads from the top to cowl sides within side wall boundary layers as well as the top wall ones, and the flame is stabilized over a wide range, which can be said to be the FA mode. Moreover, the combustion region is roughly divided into two regions: the top wall and cowl side regions.

The PA mode is due to the essentially low self-ignition of E1 engine, and even if the fuel ignites inside the engine, it is located far from the main injector. One of highly combustible regions is in the wake of the strut on the top wall side. Therefore, the principal combustion region for the PA mode is formed by that only the fuel flowing near the top wall ignites and the flame is stabilized due to the impingement

of a shock wave emanating from the cowl leading edge. In this case, the Mach number distribution shows that large subsonic regions are formed near the top wall, downstream of the D. C. section. This is because the sound of speed increases with increasing temperatures due to combustion, and not because of a large boundary layer separation. Note that a small separation exists in the corner between the top and side walls.

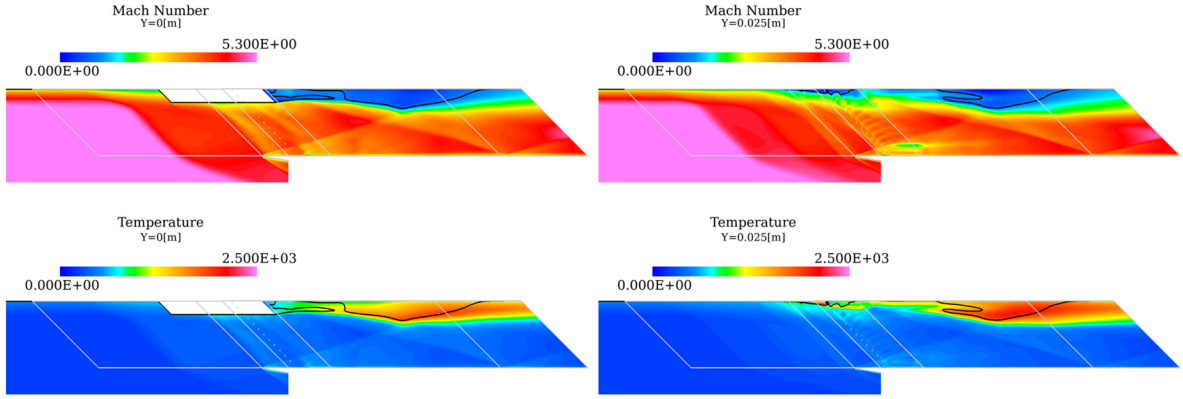

(a) Case A (left: y=0 m, right: y=0.025 m, top: Mach number, bottom: temperature [K])

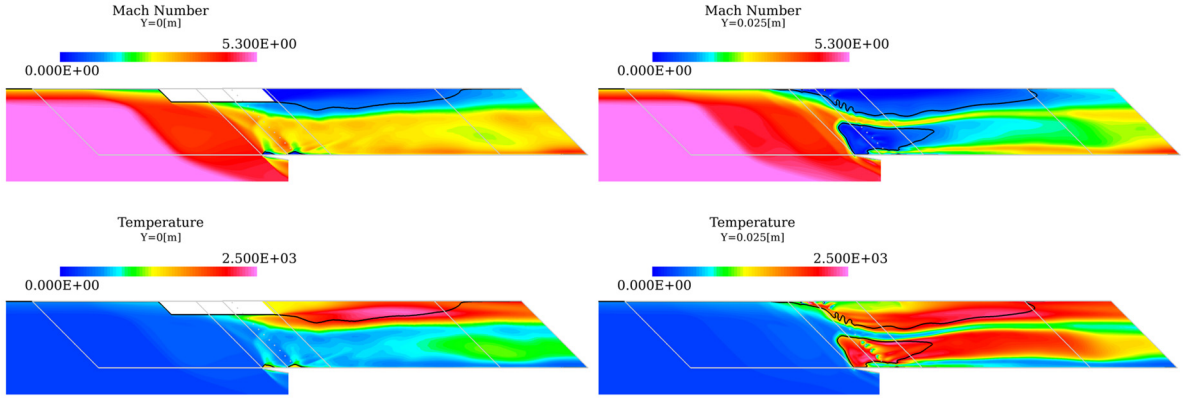

(b) Case C (left: y=0 m, right: y=0.025 m, top: Mach number, bottom: temperature [K])

Fig 3. Distributions of Mach number and temperature on y constant surface

On the other hand, the FA mode is caused by the transition from the PA mode. The trigger is that the combustor wall temperature increases and the fuel within the side wall boundary layer on the cowl side ignites. And then, through the mutual interaction between the growth of boundary layer separation and the mixing and combustion within it [15], eventually the combustion within the top wall boundary layer is also enhanced, resulting in the FA mode. Also in this case, the Mach number distribution shows large subsonic regions, which appear from the strut trailing edge to nozzle entrance on the y=0 m plane. In addition, on the y=0.025 m plane, they exist in the C. C. and D. C. sections as well as near the cowl leading edge. These subsonic regions contain recirculation zones, suggesting that they are due to a boundary layer separation. Note that thermal choking didn't occur because of no subsonic region covering all over the cross-section of flow path.

The flame on the top wall side in the PA and FA modes is stabilized mainly by the pilot fuel flame, while the flame on the cowl side in the FA mode is stabilized mainly by the boundary layer separation, and recirculation zones behind the step. To explain this, the distributions of OH mass fraction and Takeno's Flame Index [16] on an iso-surface of local equivalence ratio (φ)=1 for Case A and C are shown in Fig. 4. The Flame Index (G_{FO}) is defined as:

$$G_{FO} = \nabla Y_{H_2} \cdot \nabla Y_{O_2} \tag{1}$$

According to the definition, when G_{FO} is positive, the flame is the premixed flame, whereas when it is negative, the flame is the diffusion flame.

For the PA mode (Case A), positive G_{FO} regions, where OH is produced just in the downstream, exist on the top wall side in the D. C. section, suggesting a premixed flame region. This is because the fuel doesn't ignite just after the injection and the fuel/air mixing proceeds until the premixed gas is made. On the other hand, the premixed flame is also found around the region between the strut and side wall, since the pilot fuel rapidly mixes with the air to be a premixed gas because of its small amount, and it is burned by the PJ igniter. This premixed flame ignites the fuel from the main injector and holds the downstream premixed flame by providing its radicals, even though it is weakened by expansion waves originated from the strut trailing edge.

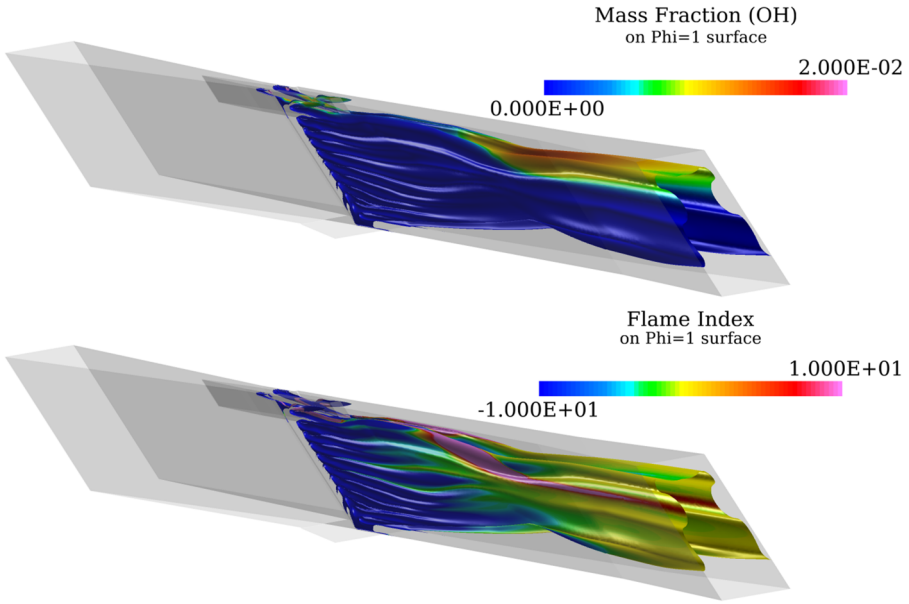

(a) Case A

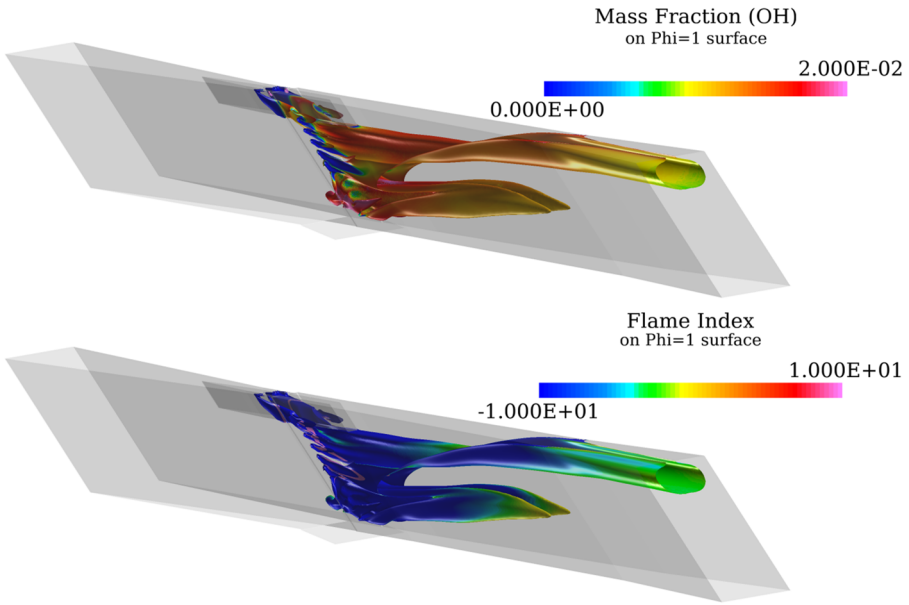

(b) Case C

Fig 4. Distributions of OH mass fraction (top) and Flame Index (bottom) on iso-surface of φ=1

For the FA mode (Case C), the diffusion flame is dominant. However, the premixed flame is found in the jet wake from the main injector on the top wall side, and the combustion is held from there due to the connection with the upstream pilot flame. On the other hand, for the combustion region on the

cowl side, the OH distribution exists in the separated boundary layer on the side wall and recirculation zone behind the step, and the combustion is held from there.

Once after the transition to the FA mode at $T_{wc} = T_{ad}$, even if T_{wc} is changed to 300 K at which usually it is the PA mode, the combustion is maintained, showing hysteresis. Fig. 2 shows almost the same thrust level between Case C and E, although it is slightly smaller for Case E. This feature is the same, even if the airflow is the V mode. This is because the combustion region on the cowl side is maintained by the recirculation zone, even if the wall temperature is decreased. Hence, the combustion region on the top wall side is also maintained, as long as the PJ igniter is turned on.

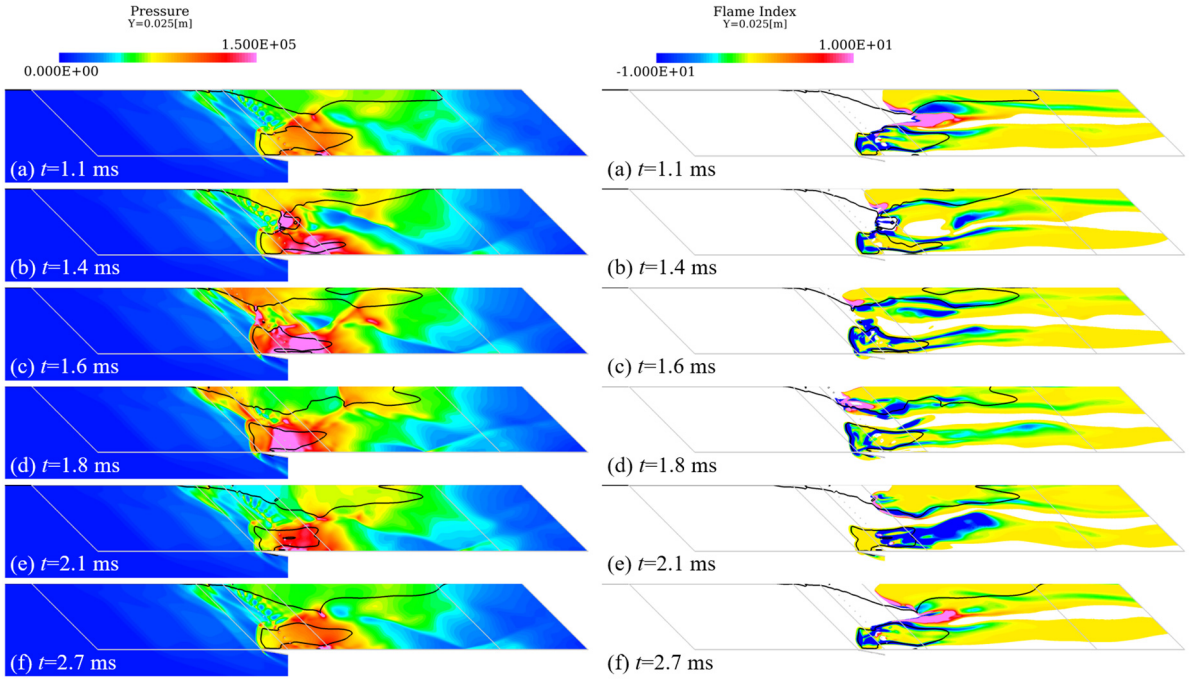

Fig 5. Left: pressure [Pa] distributions on y=0.025 m plane (CaseK)

Fig 6. Right: Flame Index distributions on y=0.025 m plane (CaseK)

3.2. Partially-blow-off mode

In Fig. 2, at the beginning, the tendency of ΔF for Case I, where the conditions include the airflow of V mode, the PJ-off, and $T_{wc} = T_{ad}$, is the same as that for Case D; after t=3 msec, however, the combustion mode is suddenly changed to the FA mode. In addition, ΔF oscillates and the solution is not converged to steady flows after all. Moreover, for Case K at T_{wc}=300 K, the combustion mode doesn't return to the PA mode like Case F, and ΔF also oscillates with a larger amplitude than Case I. In this study, we consider such a state to be the PB mode. This is because the PJ igniter is turned off, and there is no pilot flame, which is the principal mechanism for flame holding on the top wall side, so that the flame is blown off periodically. To further investigate and explain these phenomena, for Case K, the distributions of pressure and G_{FO} on the y=0.025 m plane at t=1.1, 1.4, 1.6, 1.8, 2.1 and 2.7 msec are indicated in Fig. 5 and 6 respectively. Here sonic lines colored by black are depicted all in the figures, and combustion regions where the OH mass fraction is over 1×10^{-4} are shown by colors in Fig. 6. Note that in this case, ΔF increases from t=1.1 to 1.6 msec, and then decreases from t=1.6 to 2.1 msec, being followed by remaining relatively constant from t=2.1 to 2.7 msec as shown in Fig. 2.

The two shock waves formed by the boundary layer separations on the top wall and the side wall near the cowl intersect each other in the middle of engine height to create high pressure regions. In addition, they contact with the premixed flame formed in the front of the combustion region within the top wall boundary layer so that combustion and boundary layer separations are induced there (t=1.1 msec). The high pressure region moves upstream as time passes because of the mutual interaction between the enhancement of combustion and the growth of boundary layer separation. Thanks to that, the combustion region on the top wall side also propagates upstream, resulting in the pressure gain near

the main injector (t=1.1~1.6 msec). However, when the high pressure region moves further upstream, the flame within it is quenched and the pressure is weaken, since the fuel is no longer supplied to it, resulting in the pressure drop near the main injector on the top wall side (t=1.8 msec). Then, the premixed flame on the top wall side can't stay there so that it is blown away to the downstream (t=1.8~2.1 msec). When it is brought to the crossing point of the two shock waves as mentioned before, the high pressure region revives in the middle of engine height (t=2.7 msec). In this way, the combustion region on the top wall side moves upstream and downstream periodically, and the flame repeats the blow-off. On the other hand, the combustion region on the cowl side is fixed at the same location relative stably due to the boundary layer separation, and the recirculation zone behind the step as mentioned before.

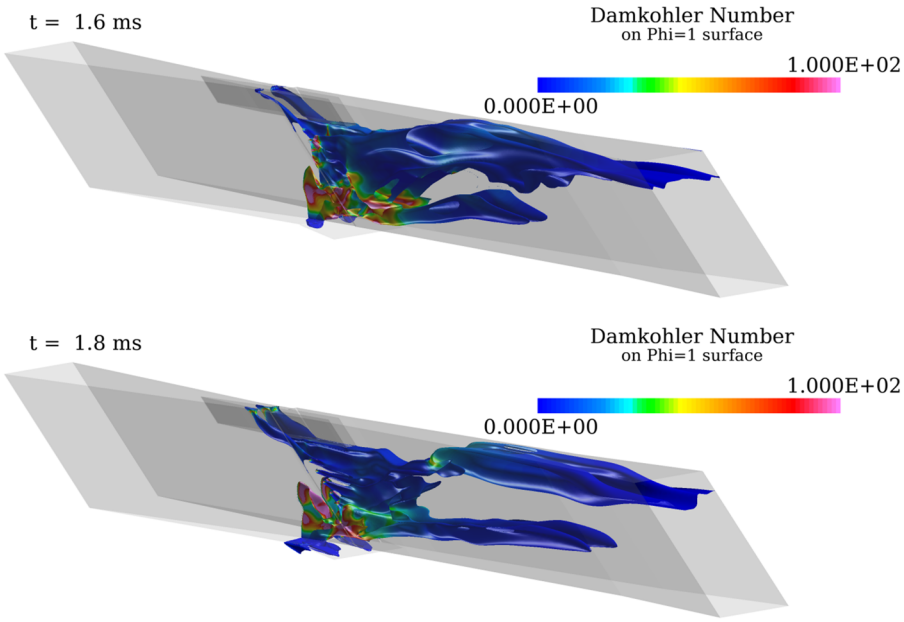

Fig 7. Damköhler number distributions on iso-surface of φ=1 (Case K)

Fig. 7 shows Damköhler number (Da) distributions on an iso-surface of φ=1, when the combustion region on the top wall side is the closest to the step at t=1.6 and 1.8 msec. The definition of Da in this study is the following form using the reaction time (τ_R) proposed by Rogers et al. [17].

$$Da = U^{-1}/\tau_R \tag{2}$$

$$\tau_R = 3.25 \times 10^{-4} p^{-1.6} exp(-0.8T/1000) \tag{3}$$

Note that the reference length for the characteristic time of flow is set to be 1 m to avoid arbitrariness and keep only a qualitative comparison. In addition, τ_R is between the times at which the temperature becomes 5 and 95 % of the difference between the initial and equilibrium ones through the one-dimensional combustion calculation. It varies only within 10 % depending on the equivalence ratio ranging from 0.5 to 1.5.

At t=1.6 msec, the fuel/air mixture at φ=1 spreads behind the step in the middle of engine height, showing high Da. This is because the high pressure region with combustion enters into this region, and the separation region upstream of the fuel jet and the recirculation region behind the step merge there. At t=1.8 msec, however, it is difficult to keep such a situation, and then, the fuel/air mixture at φ=1 disappears in the region behind the step and exists only downstream of the injector. At this time, as it is obvious from the Da distribution, the situation is changed to that it is difficult to anchor the flame near the injector. On the other hand, Da remains high on the cowl side, suggesting that the flame holding is always easier there.

3.3. Blow-off mode

In Fig. 2, for Case B, D and G, ΔF is smaller than the other cases and the combustion efficiencies at the engine exit are about 1, 4 and 1 % respectively, showing that the thrust increment is almost only

due to the momentum addition. When the PJ igniter is turned off, such a state happens; therefore, it is defined as the BO mode to contrast with the remarkable combustion occurred for the PJ-on. The cause of this state is that there is no flame holding mechanism with pilot flame at the PJ-off on the top wall side, and also the ignition and flame holding performance is low on the cowl side. For comparison of the ignition performance between the three cases, Fig. 8 shows the distributions of ignition distance (X_{ig}) [m] defined as:

$$X_{ig} = u \times \tau_{ig} \tag{4}$$

where the ignition delay time (τ_{ig}) is calculated by the following correlation, which is derived by Colket et al. [18] through experimental data.

$$\tau_{ig} = 1.6 \times 10^{-14} exp(19700/RT)[O_2]^{-1} \tag{5}$$

This correlation provides good agreement with experimental data at p=1 atm and T>1000 K.

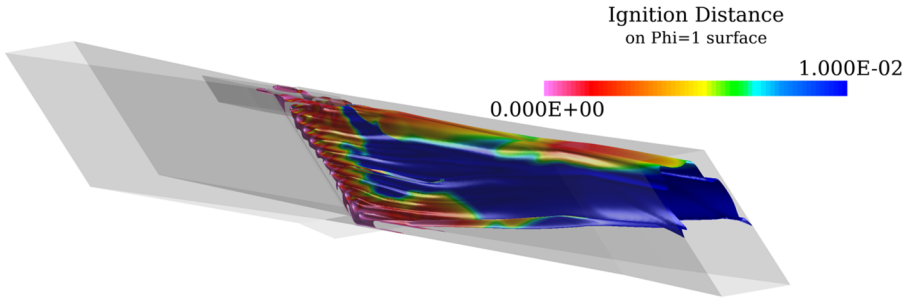

(a) Case B

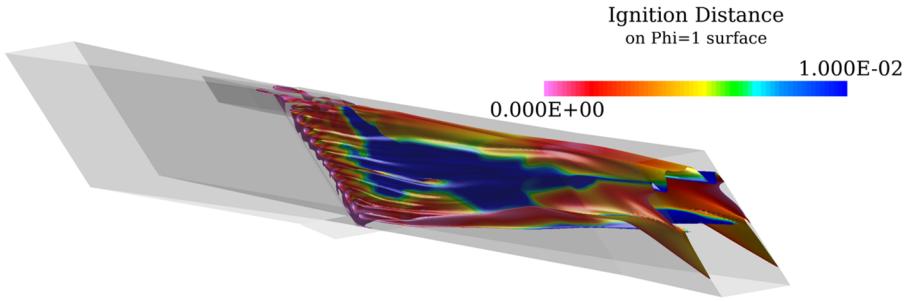

(b) Case D

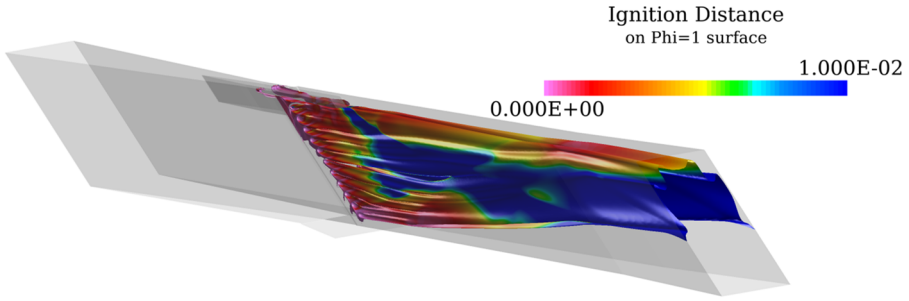

(c) Case G

Fig 8. Ignition distance [m] distributions on iso-surface of φ=1

For Case B and G, X_{ig} in the D. C. and nozzle sections, except for the region near the top wall, is much longer than the other area because of the lower temperature and pressures, and the faster flows, which are caused by the diverging of flow path. On the top wall side, X_{ig} is relatively short due to the impingement of shock waves from the strut and cowl leading edges as well as the low velocities in the boundary layer, expecting the good ignition performance; however, it is not able to hold the flame due

to no pilot flame. On the other hand, for Case D, X_{ig} becomes shorter on the cowl side downstream of the engine compared to the other two cases. This is because the temperature and pressures increase in this region by the consequence that the combustion reaction is promoted within boundary layers, where the temperature increases due to the adiabatic wall. However, the amount of combustion is small, and the combustion efficiency is also low as mentioned before. Therefore, it is impossible that the fuel reaches the recirculation zone behind the step, due to the growth of separation, which is caused by combustion, resulting in the no flame holding.

Note that comparing between Case B and G, X_{ig} is slightly shorter for Case G due to the higher total temperature in the V mode, although both the distributions are similar overall. Therefore, for Case I in the V mode, in contrast to Case D, the ignition and combustion occur closer to the injector on the cowl side due to the synergy effects that are the higher wall temperature and total temperature. Finally, through the mutual interaction between the combustion and boundary layer separation, the flame holding mechanism is established, resulting in the transition to the PB mode producing the large thrust.

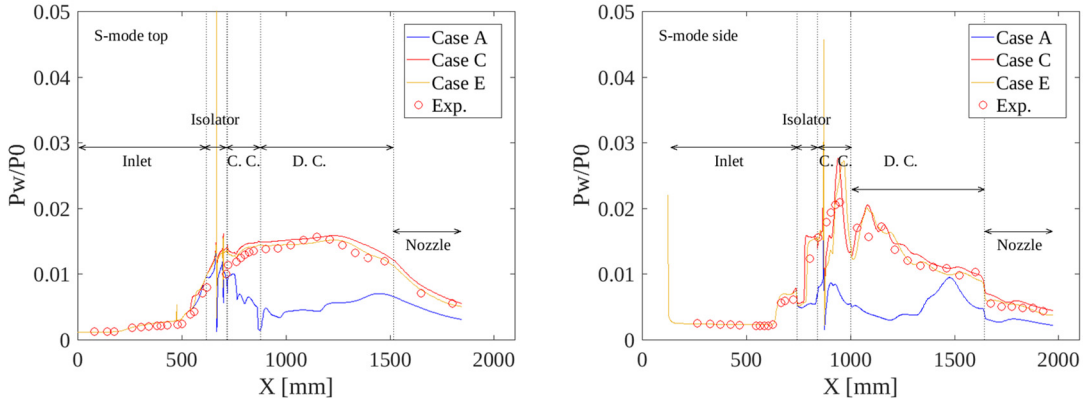

(a) S mode (left: top wall center line, right: side wall center line)

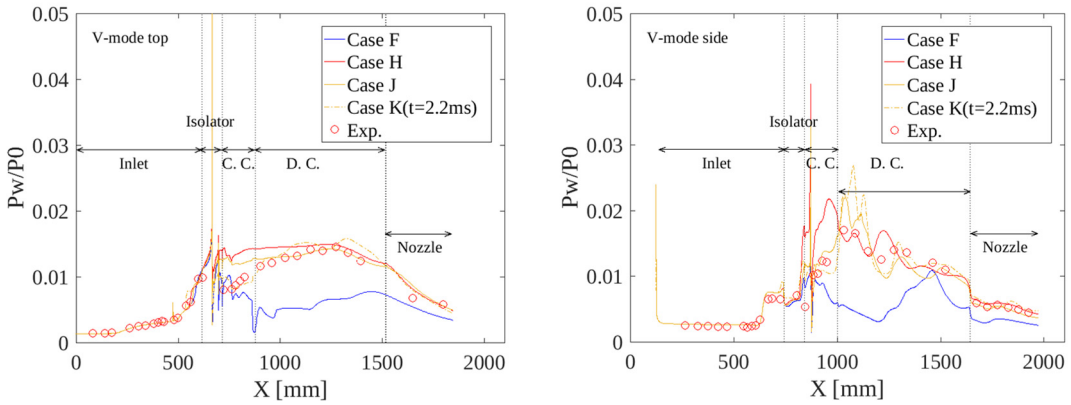

(b) V mode (left: top wall center line, right: side wall center line)

Fig 9. Comparison between CFD and RJTF results on wall pressure distributions

3.4. Comparison with RJTF test results

Fig. 9 shows the comparison between the CFD and RJTF results in terms of wall pressure distributions along the top and side wall center lines. Here the wall pressure is normalized by the incoming freestream total pressure and the top wall distributions are located at y=0.025 m in the section of strut. In addition, for the CFD results, all the combustion modes except the BO mode are shown, and for the PB mode, only the result for Case K at t=2.2 msec is shown. Note that usually the PJ igniter didn't work in the RJTF tests.

For the airflow of the S mode, the phenomena that were called the intensive combustion in the past studies correspond to the FA mode in this study. Fig. 9 shows that the wall pressure distributions for

the FA mode (Case C and E) obtained from CFD well agree with the RJTF data. On the other hand, the phenomena that were called the weak combustion in the past studies correspond to the PA mode in this study. In Fig. 9, the result for Case A, which is the PA mode, is different from the RJTF result. However, the main combustion region includes the premixed flame, suggesting the weak combustion according to the study of Kouchi et al. [6]. The result for Case F, whose airflow is the V mode, also corresponds to the weak combustion like that for Case A.

When the airflow is the V mode, the phenomena that the reaction delay was significant even in the intensive combustion mode in the past studies correspond to the PB mode. In Fig. 9, the CFD results for Case H and J, which are the FA mode, show differences with the RJTF data in terms of the pressure decrease in the C. C. section, which were typically observed in the V mode. On the other hand, the result for Case J shows good agreement with the RJTF data in terms of the onset of pressure raise due to combustion along the side wall center line, while it underestimates the pressure decrease in the C. C. section along the top wall center line. Moreover, the result for Case H is not able to predict the delay of pressure rise obtained from the RJTF tests along the side wall center line. Note that in the RJTF test for this condition, the PJ igniter didn't work properly. Therefore, the combustion mode in this case corresponds to the PB mode that occurs when the large thrust is produced without working of the PJ igniter. Actually, for Case K as shown in Fig. 9, the wall pressure distributions at some instant time agree with those obtained from the RJTF test. Note that it was difficult for the RJTF test to detect the pressure fluctuation over at 500 Hz, which is obtained from the CFD results for the PB mode because of the limitation of sampling frequency and the response delay.

4. Conclusion

Three-dimensional CFD analysis, which corresponds to Mach 6 combustion tests for a JAXA's research hydrogen fueled engine called E1, was conducted by using RANS. At a fuel equivalence ratio of 0.3, various combustion modes were observed through the computation of 11 cases, which combine different parameters including the combustor wall temperature, working of igniter (Plasma Jet: PJ igniter), airflow mode, and initial conditions. Here, the S mode is when the airflow does not contain water vapor, and the V mode is when it contains water vapor. The combustion modes were classified into 4 groups: Partially-anchored (PA), Fully-anchored (FA), Partially-blow-off (PB), and Blow-off (BO) in the view of the flame holding point, and each was examined in detail. The characteristics for each combustion mode were summarized as follows.

The PA mode:

- It occurs when the PJ igniter is turned on and the wall temperature is low.
- The principal combustion region exists only within the top wall boundary layer downstream of the engine. This is due to the essentially low self-ignition of E1 engine.
- The flame from the pilot fuel is the main factor of flame holding.

The FA mode:

- It occurs when the PJ igniter is turned on and the wall temperature is high.
- The principal combustion region exists over a wide range, and it is roughly divided into two regions: the top wall and cowl side regions. This is due to the transition from the PA mode, which is triggered by that the wall temperature increases and the fuel within the side wall boundary layer on the cowl side ignites.
- For the combustion region on the top wall side, the flame from the pilot fuel is the main factor of flame holding, while for that on the cowl side, separated boundary layers, and recirculation zones behind the step are the main factor of flame holding.
- It is maintained even if the wall temperature is decreased, because the combustion region on the cowl side is held by the recirculation zone.

The PB mode:

- It occurs when the PJ igniter is turned off, the airflow is the V mode, and the wall temperature is high.

- Due to the PJ-off, there is no pilot flame, which is the flame holding mechanism in the combustion region on the top wall side, so that the flame repeatedly blows off in that region.
- Like the FA mode, it is maintained even if the wall temperature is decreased.

The BO mode:

- It occurs when the PJ igniter is turned off and the wall temperature is low, or when the PJ ignitor is turned off, the wall temperature is high, and the airflow is the S mode.
- The cause of this state is that there is no flame holding mechanism with pilot flame at the PJ-off on the top wall side, and also the ignition and flame holding performance is low on the cowl side.

Also, the correspondence between the phenomena observed in the RJTF test and each combustion mode obtained from the CFD results is as follows.

- The phenomena that were called the intensive combustion in the past studies correspond to the FA mode.
- The phenomena that were called the weak combustion in the past studies correspond to the PA mode.
- The phenomena that the reaction delay was significant even in the intensive combustion mode in the past studies correspond to the PB mode.

References

1. RJTF Construction Group: Ramjet Engine Test Facility (RJTF), NAL TR-1347, in Japanese (2001).
2. Mitani, T., Tomioka, S., Kanda, T., Chinzei, N., Kouchi, T.: Scramjet performance achieved in engine tests from M4 to M8 flight conditions, AIAA Paper 2003-7009 (2003).
3. Kanda, T., Hiraiwa, T., Mitani, T., Tomioka, S., Chinzei, N.: Mach 6 testing of a scramjet engine model, J. of Prop. Power 13 (4), 543-551 (1997).
4. Mitani, T., Hiraiwa, T., Sato, S., Tomioka, S., Kanda, T., Tani, K.: Comparison of scramjet engine performance in Mach 6 vitiated and storage-heated air, J. of Prop. Power 13 (5), 635-642 (1997).
5. Tomioka, S., Hiraiwa, T., Kobayashi, K., Izumikawa, M., Kishida, T., Yamasaki, H.: Vitiation effects on scramjet engine performance in Mach 6 flight conditions, J. of Prop. Power 23 (4), 789-796 (2007).
6. Kouchi, T., Masuya, G., Mitani, T., Tomioka, S.: Mechanism and control of combustion-mode transition in a scramjet engine, J. of Prop. Power 28 (1), 106-112 (2012).
7. Kodera, M., Tomioka, S.: Investigation of air vitiation effects on scramjet engine performance, Proc. of 32nd Int. Symp. on Space Tech. Sci., 2019-a-49 (2019).
8. Kodera, M., Sunami, T., Nakahashi, K.: Numerical analysis of scramjet combusting flows by unstructured hybrid grid method, AIAA Paper 2000-0886 (2000).
9. Wada, Y., Liou, M.-S.: A flux splitting scheme with high-resolution and robustness for discontinuities, AIAA Paper 94-0083 (1994).
10. Spalart, P. R., Allmaras, S. R.: A one-equation turbulence model for aerodynamic flows, AIAA Paper 92-0439 (1992).
11. Spalart, P. R.: Trends in turbulence treatments, AIAA Paper 2000-2306 (2000).
12. Stahl, G., Warnatz, J.: Numerical investigation of time dependent properties and extinction of structure of methane and propane air flame-lets: Comb. Flame 85, 285-299 (1991).
13. Takita, K.: Ignition and flame-holding by oxygen, nitrogen and argon plasma torches in supersonic airflow, Comb. Flame 128, 301-313 (2002).

14. Pointwise, Version 18.1 Release 1, Pointwise, Inc., https://www.pointwise.com.
15. Sunami, T., Kodera, M., Nakahashi, K.: Considerations on mixing and combustion of a scramjet engine -transition processes from weak to intensive combustion mode, Japan Soci. Aero. Space Sci. 50 (576), 251–257, in Japanese (2002).
16. Yamashita, H., Shimada, M., Takeno, T.: A numerical study of flame stability at the transition point of jet diffusion flames, Proc. of Comb. Inst. 26, 27-34 (1996).
17. Rogers, R. C., Schexnayder, C. J.: Chemical kinetic analysis of hydrogen-air ignition and reaction times, NASA TP-1856 (1981).
18. Colket, M. B., Spadaccini, L. J.: Scramjet fuels autoignition study, J. of Prop. Power 17 (2), 315-323 (2001).